Processing and Application of Ceramics 16 [3] (2022) 251–258
https://doi.org/10.2298/PAC2203251J

Fabrication of Al_2O_3-Nb_2O_5-LiF-ZrO_2 FGMs by SPS method: Microstructural evaluation, dynamic and sintering behaviour

Paulo Roberto Rodrigues de Jesus[1], Pedro Henrique Poubel Mendonça da Silveira[1,*], Matheus Pereira Ribeiro[1], Thuane Teixeira da Silva[1], Vera Lúcia Arantes[2], Alaelson Vieira Gomes[1]

[1]*Military Institute of Engineering - IME, Department of Materials Science; Praça General Tibúrcio, 80, Praia Vermelha, Urca, 22290-270, Rio de Janeiro, RJ, Brazil*
[2]*Department of Materials Engineering, São Carlos School of Engineering, University of São Paulo, Avenida Trabalhador São-carlense 400, 13560-970 São Carlos, SP, Brazil*

Received 15 February 2022; Received in revised form 20 May 2022; Accepted 18 August 2022

Abstract

For the first time, alumina functionally graded materials (FGMs) with additions of niobium oxide, lithium fluoride and zirconia were produced by spark plasma sintering (SPS) and their sintering behaviour and dynamic properties were studied aiming to evaluate possibility of their use as ballistic shielding. Six groups of alumina samples with different layer compositions were produced by SPS at 1400 °C/5 min. The samples were characterized by dilatometry, scanning electron microscopy (SEM) and Hopkinson split bar method. The composition with the zirconia addition exhibited lower shrinkage rates at higher temperatures than the groups without zirconia, which promoted small sample shrinkage, resulting in lower density and higher porosity. The dynamic test showed that the alumina FGMs with layer containing LiF had the highest strain and strain rate values, exhibiting that the presence of continuous gradients in the composition positively affects the ceramic properties. Densification, layer change and cracks propagating through the material layers were also analysed by SEM analyses.

Keywords: *functionally graded materials, alumina, spark plasma sintering, dynamic behaviour*

I. Introduction

Functionally graded materials (FGMs) are heterogeneous materials, characterized by multi-phase properties that vary gradually (i.e. microstructure and mechanical properties, etc.). Heterogeneous materials refer to objects with different material compositions or structures. Some of the most common applications of FGMs are sensors, solar panels, semiconductors, refractories, automobiles, etc. [1–3].

Currently, ceramics have predominantly been used as a protective material for protective applications such as helicopters, armoured vehicles and bulletproof vests [4,5]. Several types of research have verified that ceramics have low density, high strength and high hardness, but are prone to crack growth, thus influencing their practicality. Therefore, new studies began to explore materials to increase the toughness of ceramics [6–8]. A known fact is that the increase in the toughness of ceramics usually decreases its strength. However, advances in research involving ceramics allowed the hardening of ceramics combined with an increase in ballistic resistance [9].

The use of ceramic FGMs in ballistic applications is a potential opportunity for improving the original properties of ceramics. From the compositional variation and microstructural control along the thickness or volume of the ceramics, the variations in properties can lead to the development of new materials that can produce lighter protection equipment and are resistant to ballistic impacts [10].

Since 2001, the US Department of Defence has allocated a large annual budget for FGMs research to develop lighter and stronger protective equipment. Custom morphologies and structural properties, such as

*Corresponding author: tel: +55 21986193395
e-mail: *pedroo.poubel@gmail.com*

physical and mechanical gradients of specific direction, make FGMs stand out among all composites. In terms of choice of armour materials, FGMs also have the following merits: FGMs have better impact performance than anti-multiple projectiles composites, as the gradient structure can reduce the impedance mismatch of different materials; the existence of a gradient structure can alter the propagation and reflection of the shockwave [11]; FGMs have an increased resistance to crack growth behaviour [12]. Several experimental approaches have been applied in the investigation of FGMs in ballistic applications, including fabrication methods, impact response, ballistic testing, crack propagation etc. [13]. The most common methods in the fabrication of ceramic FGMs are spark plasma sintering (SPS) and hot pressing (HP), techniques that enable good sinterability of advanced ceramics [14–17].

Alumina is one of the most used ceramics in ballistic protection, as it has a low cost and does not require complex processing [18]. Studies on FGMs for ballistic protection have advanced in recent years, where a study of the dynamic properties of these materials has been performed to evaluate the performance of ceramics at high strain rates (above $10^4\ s^{-1}$) [19–21]. However, the studies mostly contemplate ceramics such as TiB_2, SiC, AlN and Si_3N_4, therefore, there are few reports on the alumina-based FGMs aiming at ballistic application.

In the current study, the production and characterization of FGM samples based on alumina reinforced with niobium oxide, zirconia and lithium fluoride were investigated taking into account the variation of layers along with the material thickness. The main motivation of the study was to investigate sintering behaviour of the alumina based FGMs and their response to the dynamic test, as well as to evaluate a potential FGM for a future ballistic application.

II. Experimental

2.1. Raw materials

In this study, Al_2O_3 powder (Treibacher Scheifmittel) was used as a matrix material for the FGMs and Nb_2O_5 (Companhia Brasileira de Metalurgia e Mineração - CBMM), LiF (Dinânica) and ZrO_2 (Tosoh Corporation) were used as sintering additives. PEG (Vetec) was used to give mechanical strength to green bodies. The starting materials were used to prepare 4 different alumina-based compositions (Table 1).

2.2. Samples processing

The corresponding amounts of raw materials were mixed in an alumina jar. Deionized water in a 1:1 ratio with the precursor mixtures was used to facilitate homogenization, in addition to the insertion of alumina balls used for better powder comminution. Milling and mixing were carried out in a ball mill for a period of 8 h, followed by drying at 80 °C for 48 h. The mixtures were manually de-agglomerated using a pestle and mortar and sieved with a 42-mesh sieve to obtain the desired particle size.

The samples were sintered using a spark plasma sintering (SPS) apparatus (model SPS – 211 LX, DR. Sinter Lab™). Scheme of SPS process is shown in Fig. 1a. Six groups of alumina based FGMs were produced using different compositions given in Table 1. The groups have 1 to 4 layers with compositional variation across layers, as shown in Table 2.

The powders were inserted into a graphite mould (⌀10 mm) and the FGMs samples were prepared according to scheme shown in Figure 1b. Ceramic disks

Table 1. Sample compositions

Composition	Al_2O_3 [wt.%]	Nb_2O_5 [wt.%]	LiF [wt.%]	ZrO_2 [wt.%]
1	96.00	4	-	-
2	95.75	4	0.25	-
3	95.50	4	0.50	-
4	92.48	-	-	7.52

Table 2. Definition of alumina based FGM groups

Group	Number of layers	Composition (Table 1)	Thickness [mm]
F-C1	1	1	6
F-C3	1	3	6
F-C1/3	2	1/3	3
F-C1/2/3	3	1/2/3	2
F-C1/3/4	3	1/3/4	2
F-C1/2/3/4	4	1/2/3/4	1.5

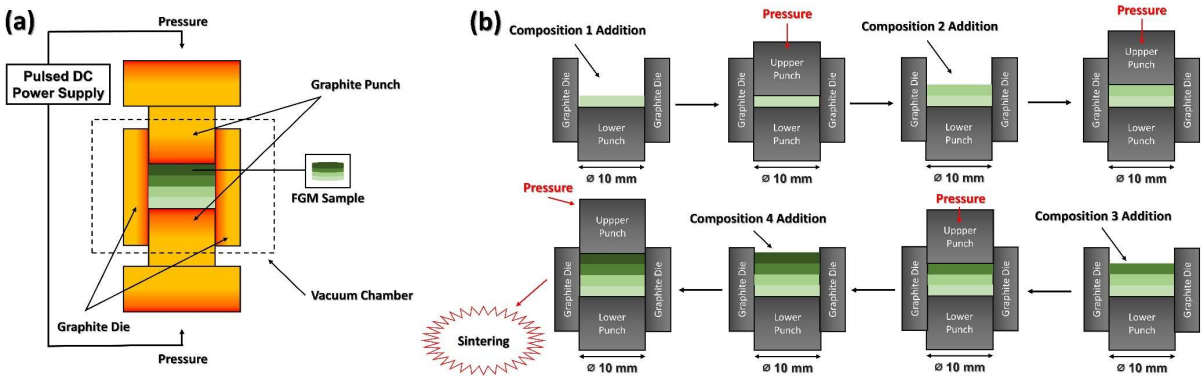

Figure 1. Schematic of SPS process (a) and used steps in the preparation of FGM samples

with total mass of 2 g were produced, divided equally between the layers of the FGMs. Initially, the powders of the first composition were inserted into the graphite die, then the upper punch of the die was pressed lightly against the powders to compact them. The upper punch was removed and the second composition was inserted on top of the first, followed by another pressure. The same procedure was performed for the groups with 3 and 4 layers. After insertion of all compositions into the mould, a pressure of 50 MPa was applied to the mould, coupled with other parameters such as sintering time of 5 min and sintering temperature of 1400 °C. The heating rate was 65 °C/min. The current was turned off according to the retention time and the cooling rate corresponds to the natural cooling of the furnace. Subsequently, the samples, having thickness of 6 mm and diameter of 10 mm, were removed from the graphite mould.

2.3. Characterization

The bulk density measurements were conducted on the sintered samples using Archimedes' principle, using an analytical balance with an attached density kit. The bulk density of the samples (ρ) was obtained by Eq. 1:

$$\rho = \frac{M_{dry}}{M_{dry} - M_{wet}} \cdot \rho_{liquid} \tag{1}$$

where M_{dry} and M_{wet} are masses of the sintered samples in air and liquid, respectively, and ρ_{liquid} is the density of water at room temperature.

The porosity (P_0) of sintered samples was obtained by employing Eq. 2:

$$P_0 = \frac{m_2 - m_1}{m_2 - m_3} \cdot 100 \tag{2}$$

where, m_1, m_2 and m_3 are mass of the samples weighed after drying, mass of wet sample in air and mass of the sample in liquid, respectively.

Dilatometric studies were performed in a dilatometer (Netzsch, DIL, 402 E/7) with a 5 °C/min heating rate up to 1500 °C/1 h, in flowing argon (1 atm) followed by cooling with a rate of 10 °C/min.

The fractured surfaces of the samples were analysed using a Quanta FEG 250 FEI SEM microscope (Hillsboro, USA). The equipment was used with secondary electrons (SE) and back-scattered electrons diffraction (BSED) detectors at an acceleration voltage of 15 and 30 kV, respectively. The fractured samples were coated with gold in the Leica Ace600 equipment (Wetzlar, Germany).

The Hopkinson bar consists of an incident bar and a transmitter bar, with a specimen placed between them and a striker bar that produces an impact on the incident bar to generate a longitudinal compressive pulse that propagates towards the specimen (Fig. 2) [22]. The pulse is partially reflected at the border of the incident bar and partially transmitted through the specimen. In this case, the diametral loading generates tension perpendicular to the load plane, which eventually causes the specimen to split [23].

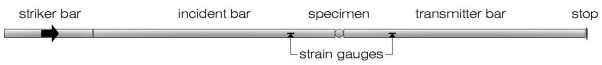

Figure 2. Schematic of a split Hopkinson pressure bar with high-strength steel bars

The strain records of the incident, reflected and transmitted pulses are used to calculate the corresponding stress pulses and the tensile stress in the loading plane, which are derived from Eq. 3:

$$\sigma = \frac{2P}{\pi \cdot W \cdot D} \tag{3}$$

where P is the load transmitted through the cylinder and W and D are respectively the width and diameter of the cylinder. P is in turn calculated from the transmitted stress. The strain rate $\dot{\varepsilon}$ is obtained using Eq. 4:

$$\dot{\varepsilon} = \frac{\mathrm{d}\varepsilon}{\mathrm{d}t} \tag{4}$$

where $\mathrm{d}\varepsilon$ is the derivative of the deformation obtained from the dynamic test and the derivative is restricted to the linear ramp-up of the stress history.

III. Results and discussion

3.1. Sintering behaviour

Linear shrinkages of all the samples, determined from dilatometric experiments, are shown in Fig. 3. It can be seen that at the dwell temperature (1500 °C) there is no shrinkage, indicating that the densification process in all samples at this temperature is hindered. The expansion curves of the samples were similar, except for the composition 2, which had a reduction in its softening point at 763 °C (Fig. 3b), where the onset of shrinkage occurred at 956 °C and its maximum retraction point occurred at 1171 °C. For the composition 1, the maximum shrinkage peak appeared at 1239 °C. The composition 3, which presents only a variation in the LiF content, compared to the composition 2, exhibits a decrease in temperature where the maximum shrinkage peak occurs, appearing at 1140 °C. The composition 4 showed the beginning of the shrinkage process at 1095 °C, reaching its maximum point at the end of the test (1470 °C). The retraction of the composition 4 occurred at a temperature lower than that reported by Surzhikov *et al.* [24] who found in their work the maximum shrinkage for Al_2O_3-ZrO_2 at T = 1550 °C.

Figure 4 shows the evolution of shrinkage during SPS process, recorded *in situ* for the different FGM groups. Observing the shrinkage curves during sintering, it can be seen that with the increase of temperature, shrinkage of the ceramic samples also increases. The shrink-

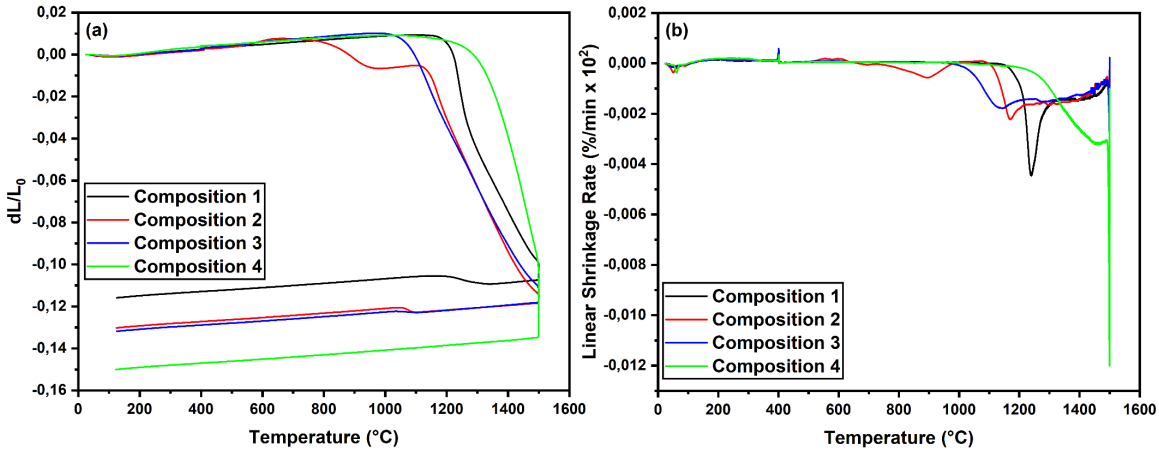

Figure 3. Dilatometric results: a) linear shrinkage versus temperature and b) linear shrinkage rate versus temperature

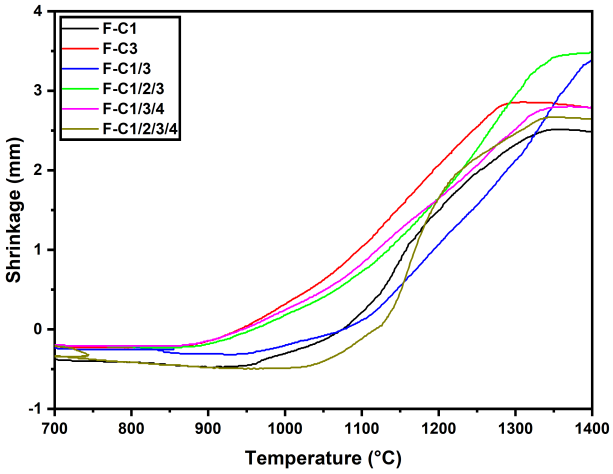

Figure 4. Shrinkage curves recorded during SPS processing

age of the ceramic samples F-C1, F-C3, F-C1/3 and F-C1/2/3 were stabilized in the temperature range between 1250 and 1300 °C. The samples F-C1/3/4 and F-C1/2/3/4 showed a greater retraction during sintering, which can harm the interface of the FGM layers. It is reported in the literature that in order to reduce the tension between layers in FGM processing, a smoother transition in the composition between adjacent layer is necessary to prevent excessive shrinkage from generating tensions that can cause cracks and reduce and harm the performance of the material [25]. Table 3 shows the results of the density and porosity of the analysed groups of FGMs.

The samples F-C1 and F-C3 have the highest densities among the groups analysed in this work. As the groups F-C1/3 to F-C1/2/3/4 are not homogeneous, the increase in the number of FGM layers caused a reduction in the density of these groups, even with SPS technique which allows to obtain high relative densities, close or equal to the theoretical densities of the materials. SPS technique allowed a high densification of the group F-C1, which presented a density higher than the value found in the work of Gomes *et al.* [26]. They prepared alumina ceramics with similar composition, but used uniaxial cold press and pressureless sintering. The F-C3 group has density similar to the F-C1. The addition of LiF as a sintering additive had no significant effect on the densification of the Al_2O_3-Nb_2O_5 composite, opposite to the literature data, which reported an increase in densification with small additions of LiF [27,28]. However, the values obtained through SPS are higher than the results obtained by Santos *et al.* [27] and Silveira *et al.* [28], where both works used the same composition of the F-C3 group.

To obtain higher densities of Al_2O_3 with SPS technique, it is necessary to make adjustments to the adopted pressure. Wang *et al.* [29] reported in their study that the increase in internal pressure using SPS technique results in a gain in alumina densification, obtaining values close to the theoretical density. The dwell time at the sintering level also affects the relative density of Al_2O_3.

The FGMs samples (groups F-C1/3, F-C1/2/3, F-C1/3/4 and F-C1/2/3/4) showed a reduction in density when compared to the F-C1 and F-C3 groups. The increase in the number of layers resulted in a density reduction of the FGMs, as observed for the F-C1/2/3/4 sample, which has relative density of 88.32 %TD. Dur-

Table 3. Bulk density ρ, theoretical density ρ_{theo}, relative density ρ_r and porosity P_0 of FGMs sintered samples

Group	ρ [g/cm^3]	ρ_{theo} [g/cm^3]	ρ_r [%TD]	P_0
F-C1	3.78 ± 0.11	3.98	95.07 ± 2.76	0.69 ± 0.03
F-C3	3.77 ± 0.14	3.97	95.00 ± 3.82	0.90 ± 0.04
F-C1/3	3.59 ± 0.02	3.97	90.35 ± 0.50	1.87 ± 0.01
F-C1/2/3	3.61 ± 0.08	3.97	90.91 ± 2.02	0.83 ± 0.02
F-C1/3/4	3.62 ± 0.09	4.02	90.07 ± 2.24	1.55 ± 0.02
F-C1/2/3/4	3.54 ± 0.14	4.01	88.32 ± 3.58	1.44 ± 0.04

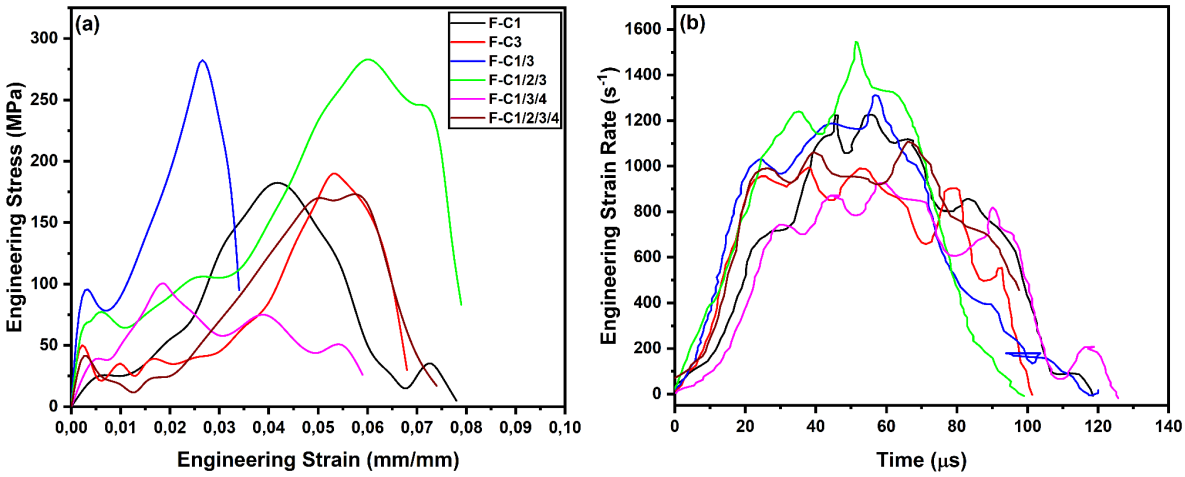

Figure 5. Dynamic stress-strain curves (a) and deformation rate curves (b)

ing the sintering, a difference in the shrinkage rates of each layer occurs, due to a difference in composition, where there is a shift from one layer to the next from the compound Al_2O_3-Nb_2O_5/Al_2O_3-Nb_2O_5-LiF to Al_2O_3-ZrO_2, producing a discontinuous gradient [30].

The F-C1 group has the lowest porosity and the F-C1/3 sample has the highest porosity in comparison to all fabricated samples. Even with this difference in porosity varying between 0.69 and 1.87%, all groups had a low amount of pores. This means that the present porosity is related to the presence of closed pores. This is an important and positive factor, as the open pores are connected to the surface, impairing the mechanical strength of ceramics, as many fractures are initiated in open pores [31].

3.2. Dynamic properties

Figure 5 shows the stress vs. strain curves and strain rate vs. time curves obtained with the Hopkinson bar method. The NBR 15000 ABNT [32] standard defines and assesses conditions for ballistic materials, where there are different levels related to weapon calibre, projectile velocity, among other criteria. Based on level III of the standard (7.62 × 51 mm ammunition), the tensile strength (σ) results obtained in the test and its deformation rate were analysed and compared. The results are shown in Table 4.

In a multi-layer shielding system, the main purpose of the ceramic material is to absorb most of the projectile's kinetic energy. For this, a combination of factors is necessary, including the mechanical strength limit measured in this case as rupture stress or fracture stress, preferably greater than 200 MPa [33]. This should be combined with the propagation of stress waves from the ballistic impact measured in the form of strain rate, preferably in the intermediate range around 1000 s^{-1} [34].

The results in Table 4 indicate that the groups F-C1/2/3 and F-C1/3 had the highest stresses among all groups, as well as the highest deformation rates. These two groups have higher stresses than those of the single-

Table 4. Maximum stress σ and maximum strain rate $\dot{\varepsilon}$ values of the FGMs obtained from the Hopkinson split bar

Group	σ [MPa]	$\dot{\varepsilon}$ [s^{-1}]
F-C1	186.83	1264.90
F-C3	190.10	1012.24
F-C1/3	282.37	1346.84
F-C1/2/3	283.08	1559.39
F-C1/3/4	106.41	930.04
F-C1/2/3/4	175.40	1118.86

layer F-C1 and F-C3 groups. The FGMs formed by different Al_2O_3-Nb_2O_5 and Al_2O_3-Nb_2O_5-LiF compositions resulted in better dynamic behaviour when compared with the single-layer materials (F-C1 and F-C3) and the FGMs with layers of Al_2O_3-ZrO_2 compounds. The addition of ZrO_2 (the groups F-C1/3/4 and F-C1/2/3/4) resulted in FGMs with low densification and lower weaker dynamic behaviour than other groups. The higher number of layers present in the material plus the addition of a layer with another compound caused a difference in the shrinkage of layers during the sintering, causing discontinuous gradients.

Internal stresses caused by the variation of mechanical and thermal properties at interfaces between two different materials can affect the implementation of FGMs. However, these stresses can be reduced and redistributed in a planned way, incorporating an intermediate layer between the two materials [35].

3.3. Microstructural analysis

SEM micrographs of the fractured surfaces of the samples are shown in Fig. 6. It is possible to observe the absence of pores between the grains of the sintered sample F-C1 (Fig. 6a). The sample F-C3, has also microstructure with high density (Fig. 6b). These two groups of samples presented a grain growth more expressed than in other groups, making the sintering of these homogeneous single-layer groups more effective. Figure 6c shows the microstructure of the sample F-C1/3 consisting of two layers with composition

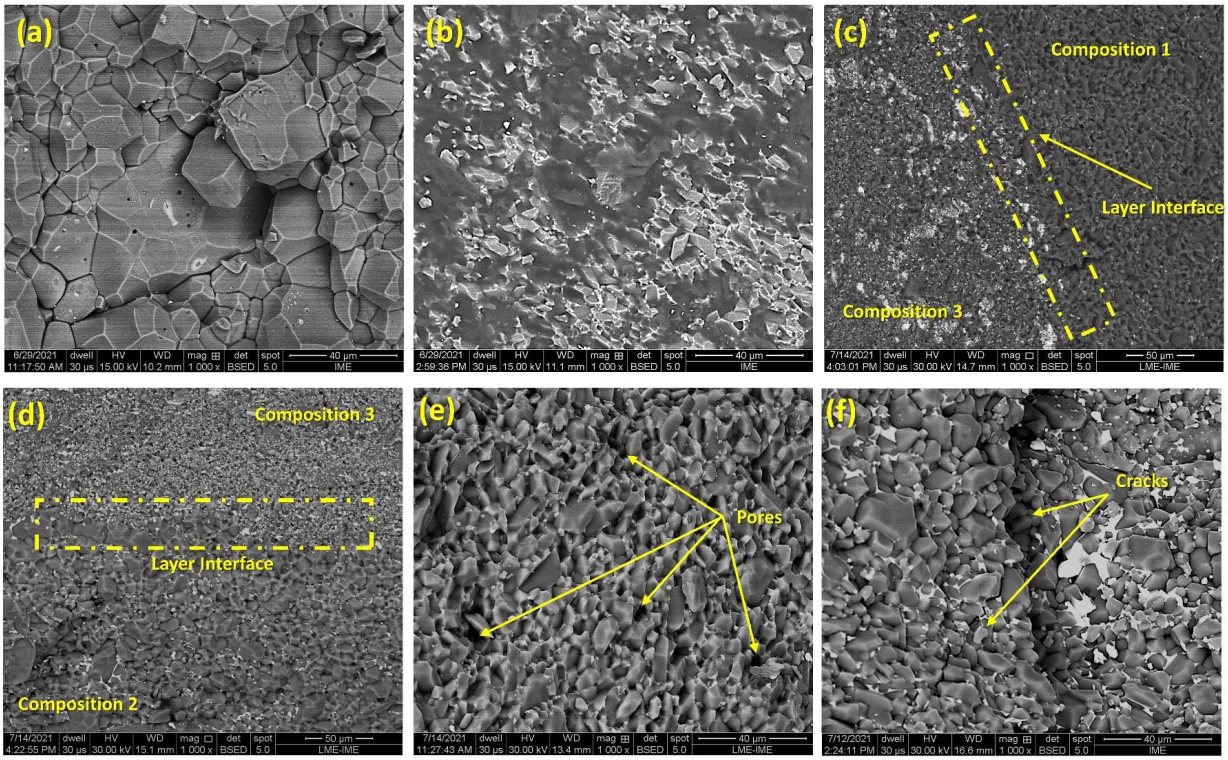

Figure 6. SEM micrographs of the fractured surfaces of the analysed samples: a) F-C1, b) F-C3, c) F-C1/3, d) F-C1/2/3, e) F-C1/3/4 and f) F-C1/2/3/4

1 (96 wt.% Al_2O_3 - 4 wt.% Nb_2O_5) and composition 2 (95.5 wt.% Al_2O_3 - 4 wt.% Nb_2O_5 - 0.5 wt.% LiF). The region with the composition 1 shows a slight increase in densification when compared to the layer with the composition 3, which shows white regions that may be an indication of the formation of $LiNbO_3$ or Nb_3O_7F, which is formed by diffusion during sintering [28,36]. The grain growth of the layer with the composition 1 is larger than the layer with the composition 3, but the grain growth was not as significant as that exhibited in the F-C1 and F-C3 groups. The different thermal contractions between the two compositions may have acted as a barrier to grain growth [37]. Figure 6d shows the microstructure of the three-layer sample F-C1/2/3. It is possible to observe the interface of the layers with the compositions 2 and 3. The region with predominance of the composition 2 (95.75 wt.% Al_2O_3 - 4 wt.% Nb_2O_5 - 0.25 wt.% LiF) presents a behaviour similar to that found in the composition 1, where grain growth occurs with the possible presence of eutectic phases (Nb_3O_7F and $LiNbO_3$) in the grain boundaries (white regions). The increase in LiF content caused a decrease in grain growth. In addition, the increase in the number of layers caused an increase in the total porosity of the sample, in which one notices the presence of small pores along the entire surface of the sample. Figure 6e shows the surface of the layer containing composition 4 (92.48 wt.% Al_2O_3 - 7.52 wt.% ZrO_2) of the three-layer sample F-C1/3/4. The combination of 3 layers with the abrupt composition change caused a high concentration of pores, as it can be seen in the SEM image. This high porosity content added to the discontinuous gradient formed by the layer change with the compositions 3 and 4 collaborated to reduce its performance in the FGM in the Hopkinson split bar test. Figure 6f illustrates the microstructure of the four-layer sample F-C1/2/3/4. In the SEM image the presence of intergranular cracks is seen, arising from internal stresses and different thermal shrinkage during sintering. The addition of 4 layers in the FGM caused an increase in the maximum stress and deformation rate, where the higher number of layers may have contributed more to this phenomenon. The inclusion of the several different layers influenced the propagation of shockwaves through the layers.

Figure 7 shows the fracture surface of the sample F-C1/2/3/4 after the Hopkinson split bar test, where the crack propagated through the layers. At the layer transition, the crack splits. In order to solve certain discontinuity problems between the layers, a potential solution is to investigate intermediate layers consisting of the compound Al_2O_3-ZrO_2-Nb_2O_5 and/or Al_2O_3-ZrO_2-LiF. The addition of these suggested compounds as an intermediate layer in the FGM could possibly minimize the effects of different thermal contractions, promoting a continuous transition in the microstructure and improving the mechanical and dynamic performance of FGMs.

IV. Conclusions

In this work, FGMs with alumina layers having different compositions, i.e. modified with Nb_2O_5, LiF, and ZrO_2, were produced. The samples were sintered by

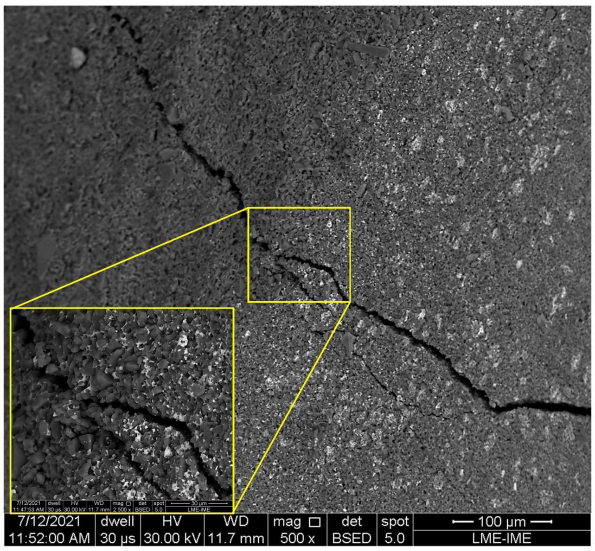

Figure 7. Intergranular crack propagation between layers in the F-C1/2/3/4 FGM sample

SPS method at a temperature of 1400 °C and tested by the Hopkinson bar method. The FGMs with two (F-C1/2/3) and three (F-C1/3) layers containing LiF showed the highest values of rupture stress and strain rate, obtaining values that are compatible with level III of NBR 15000 standard. The only group that presented a strain rate below 1000 s^{-1} was the three-layer F-C1/3/4 group, which presented a rate of 930.04 s^{-1}, not meeting the requirements of NBR 15000. The variation in the LiF content between the layers of FGMs allowed the superior performance of these 2 groups compared to others. The addition of layers with ZrO_2 caused the formation of a discontinuous gradient in the samples in the groups F-C1/3/4 and F-C1/2/3/4, reducing the material's performance. The FGMs produced in this study have the potential for application in level III bulletproof vests, meeting the requirements of NBR 15000 standard.

Acknowledgement: This study was financed in part by the Coordenação de Aperfeiçoamento de Pessoal de Nível Superior - Brasil (CAPES) - Finance Code 001. The authors are grateful to Centro Tecnológico do Exército - CTEx for their assistance with the Hopkinson bar tests. The authors thank the Universidade Estadual do Norte Fluminense (UENF) for processing FGMs using the SPS method.

References

1. V. Kumar, D. Burns, D. Dutta, C. Hoffmann, "A framework for object modelling", *Comp. Aid. Design*, **31** [9] (1999) 541–556.
2. A.J. Markworth, K.S. Ramesh, W.P. Marks Jr., "Modelling studies applied to functionally graded materials", *J. Mater. Sci.,* **30** (1995) 2183–2193.
3. M. Mohammadi, M. Rajabi, M. Ghadiri, "Functionally graded materials (FGMs): A review of classifications, fabrication methods and their applications", *Process. Appl. Ceram.,* **15** [4] (2021) 319–343.
4. A. Reyes-Rojas, H. Esparza-Ponce, S.D. De la Torre, E. Torres-Moye, "Compressive strain-dependent bending strength property of Al_2O_3-ZrO_2 (1.5 mol% Y_2O_3) composites performance by HIP", *Mater. Chem. Phys.,* **114** [2-3] (2009) 756–762.
5. P.H.P.M. Silveira, T.T. Silva, M.P. Ribeiro, P.RR. Jesus, P.C.R.S. Credmann, A.V. Gomes, "A brief review of alumina, silicon carbide and boron carbide ceramic materials for ballistic applications", *Acad. Let.,* **2021** (2021) 3742.
6. D. Blumer, D. Rittel, "The influence of microstructure on the static and dynamic strength of transparent magnesium aluminate spinel ($MgAl_2O_4$)", *J. Eur. Ceram. Soc.,* **38** [10] (2018) 3618–3634.
7. D. Hallam, A. Heaton, B. James, P. Smith, J. Yeomans, "The correlation of indentation behaviour with ballistic performance for spark plasma sintered armour ceramics", *J. Eur. Ceram. Soc.,* **35** [8] (2015) 2243–2252.
8. A.B. Dresch, J. Venturini, S. Arcaro, O.R.K. Montedo, C.P. Bergmann, "Ballistic ceramics and analysis of their mechanical properties for armour applications: A review", *Ceram. Int.,* **47** [1 part. a] (2021) 8743–8761.
9. X.F. Zhang, Y.C. Li, "On the comparison of the ballistic performance of 10% zirconia toughened alumina and 95% alumina ceramic target", *Mater. Des.,* **31** [4] (2010) 1945–1952.
10. C.Y. Huang, Y.L. Chen, "Effect of mechanical properties on the ballistic resistance capability of Al_2O_3-ZrO_2 functionally graded materials", *Ceram. Int.,* **42** [11] (2016) 12946–12955.
11. V.K. Pandey, B.P. Patel, S. Guruprasad, "Mechanical properties of Al/Al_2O_3 and Al/B_4C composites", *Adv. Mater. Res.,* **5** [4] (2016) 263–277.
12. M.T. Tilbrook, R.J. Moon, M. Hoffmann, "Crack propagation in graded composites", *Comp. Sci. Technol.,* **65** [2] (2006) 201–220.
13. A. Pettersson, P. Magnusson, P. Lundberg, M. Nygren, "Titanium-titanium diboride composites as part of a gradient armour material", *Int. J. Imp. Eng.,* **32** [1-4] (2005) 387–399.
14. L.K. Pillari, S.R. Bakshi, P. Chaudhuri, B.S. Murty, "Fabrication of W-Cu functionally graded composites using high energy ball milling and spark plasma sintering for plasma facing components", *Adv. Powder Technol.,* **31** [8] (2020) 3657–3666.
15. H. Pan, T. Song, Z. Whang, "An analytical model for collinear cracks in functionally graded materials with general mechanical properties", *Composite Struct.,* **132** [15] (2015) 359–371.
16. Y. Hou, G.H. Zhang, K.C. Chou, "Comparison of hot pressing sintering and conventional powder-sintering in preparation of CaO-Al_2O_3-SiO_2-Fe_3O_4-R_2O glass ceramics", *J. Non-Crystal. Solids,* **564** (2021) 120829.
17. Q. Dai, D. He, F. Meng, P. Liu, X. Liu, "Dielectric constant, dielectric loss and thermal conductivity of Si_3N_4 ceramics by hot pressing with CeO_2-MgO as sintering aid", *Mater. Sci. Sem. Process.,* **121** (2021) 105409.
18. M.S. Boldin, N.N. Berendeev, N.V. Melekhin,, A.A. Popov, A.V. Nokhrin, V.N. Chuvildeev, "Review of ballistic performance of alumina: Comparison of alumina with silicon carbide and boron carbide", *Ceram. Int.,* **47** [18] (2021) 25201–25213.
19. A. Kidane, A. Shukla, "Dynamic constitutive behavior of Ti/TiB FGM under thermo-mechanical loading", *J. Mater. Sci.,* **43** (2008) 2771–2777.

20. A. Kidane, A. Shukla, "Quasi-static and dynamic fracture initiation toughness of Ti/TiB layered functionally graded material under thermo-mechanical loading", *Eng. Fracture Mech.,* **77** [3] (2010) 479–491.
21. S.Y. Yang, X. Liu, D.F. Cao, H. Mei, Z.T. Lei, L.S. Liu, "A study on propagation characteristic of one-dimensional stress wave in functionally graded armor composites", *J. Phys. Conf. Series,* **419** (2013) 012046.
22. B.A. Gama, S.L. Lopatnikov, J.W. Gillespie Jr, "Hopkinson bar experimental technique: A critical review", *Appl. Mech. Rev.,* **57** [4] (2004) 223–250.
23. Sudheera, Y.S. Rammohan, M.S. Pradeep, "Split Hopkinson pressure bar apparatus for compression testing: A review", *Mater. Today Proceed.,* **5** [1 part. 3] (2018) 2824–2829.
24. A.P. Surzhikov, T.S. Frangulyan, S.A. Ghyngazov, I.P. Vasiliev, "A dilatometric study of sintering of composite ceramics manufactured from ultrafine ZrO_2(Y)–Al_2O_3 powders under different thermal-temporal firing conditions", *Russ. Phys. J.*, **57** (2014) 411–415.
25. L. Wang, C. Zhang, A. Agarwal, S. Bhusal, "Fabrication and characterization of functionally graded materials Ta10W-YSZ by SPS", *Int. J. Ref. Met. Hard Mater.*, **93** (2020) 105348.
26. A.V. Gomes, L.H.L. Louro, C.R.C. Costa, "Ballistic behavior of alumina with niobia additions", *J. Phys. IV France.,* **134** (2006) 1009–1014.
27. J.L. Santos, R.L.S.B. Marçal, P.R.R. Jesus, A.V. Gomes, E.P. Lima Jr., S. N. Monteiro, J.B. Campos, L.H.L. Louro, "Effect of LiF as sintering agent on the densification and phase formation in Al_2O_3 - 4 wt pct Nb_2O_5 ceramic compound", *Met. Mater. Trans. A.,* **48** (2017) 4432–4440.
28. P.H.P.M. Silveira, P.R.R. Jesus, M.P. Ribeiro, S.N. Monteiro, J.C.S. Oliveira, A.V. Gomes, "Sintering behavior of Al_2O_3 ceramics doped with pre-sintered Nb_2O_5 and LiF", *Mater. Sci. Forum,* **1012** (2020) 190–195.
29. S.W. Wang, L.D. Chen, T. Hirai, "Densification of Al_2O_3 powder using spark plasma sintering", *J. Mater. Res.,* **15** (2000) 982–987.
30. X. Xu, X. Hu, S. Ren, H. Geng, H. Du, J. Liu, "Fine grained Al_2O_3-ZrO_2 (Y_2O_3) ceramics by controlled crystallization of amorphous phase", *J. Am. Ceram. Soc*., **36** [7] (2016) 1791–1796.
31. D. Schueller, E.C. Bianchi, P.R. Aguiar, "Influência de defeitos e diferentes processos de fabricação nas propriedades mecânicas finais de cerâmicas", *Ceramica,* **54** [332] (2008) 435–442.
32. Associação Brasileira de Normas Técnicas – ABNT. NBR 15000: Blindagens Para Impactos Balísticos – Classificação e Critérios de Avaliação. Rio de Janeiro: ABNT, 2005.
33. O.L. Ighodaro, O.I. Okoli, "Fracture toughness enhancement for alumina systems: A review", *Appl. Ceram. Technol.*, **5** [3] (2008) 313–323.
34. B.N. Kim, K. Hiraga, K. Morita, Y Sakka, "A high-strain-rate superplastic ceramic", *Nature,* **413** (2001) 288–291.
35. B. Kieback, A. Neubrand, H. Riedel, "Processing techniques for functionally graded materials", *Mater. Sci. Eng. A*, **362** [1-2] (2003) 81–106.
36. F. Huang, H. Zhao, A. Yan, Z. Li, H. Liang, Q. Gao, Y. Qiang, "In situ thermal decomposition for preparation of Nb_3O_7F/Nb_2O_5 hybrid nanomaterials with enhanced photocatalytic performance", *J. Alloys Compd.,* **695** [25] (2017) 489–495.
37. S. Farahmand, A.S. Monazzah, M.H. Soorgee, "The fabrication of Al_2O_3-Al FGM by SPS method under different sintering temperatures: Microstructural evaluation and bending behavior", *Ceram. Int.,* **45** (2019) 22775–22782.